Inertia Welding Nickel-Based Superalloy: Part II. Residual Stress Characterization

M. PREUSS, J.W.L. PANG, P.J. WITHERS, and G.J. BAXTER

The next generation of Ni-based alloys for aeroengines are richer in γ' than existing alloys and are more difficult to weld by conventional means. Inertia welding is currently being developed as a joining technique for these alloys. Steep microstructural gradients have been observed in nickel-based superalloy RR1000 tube structures welded by inertia friction welding,[1] and in this article, the concomitant residual stresses are mapped at depth using neutron diffraction. One tube in the as-welded and two in the postweld heat-treated (PWHT) condition have been investigated. In the case of the as-welded specimen, it was necessary to establish the variation of the stress-free lattice parameter, a_0, across the weld line to infer elastic strain from lattice spacing changes. A biaxial $\sin^2\psi$ measurement on thin slices was used to determine a_0 as a function of the axial position from the weld line. This was in excellent agreement with the variation inferred by imposing a stress balance on the axial measurements. The change of a_0 across the weld line can be rationalized in terms of the observed variation in the element partitioning effect between the matrix (γ) and the precipitates (γ'). It was found that the residual stresses in the weld and heat-affected zone generated by the welding process are large, especially close to the inner diameter of the welded ring. The experimental results have shown that, in order to relax the residual stresses sufficiently, the heat-treatment temperature must be increased by 50 °C over the conventional heat-treatment temperature. This is due to the high γ' content of RR1000.

I. INTRODUCTION

THE push towards new high γ'-containing Ni-based superalloys to achieve higher operating temperatures in aeroengines has led to the development of alloys that are difficult to join by conventional means. As a solid-phase joining process, inertia welding is a promising alternative. In many ways, it resembles a localized forging process. Because of the localized heat generation caused by the friction process and the very severe cooling rates, significant residual stresses are introduced. In part I,[1] the metallurgical development of nickel-based superalloy, RR1000, in the near-weld region has been described. RR1000 has a high volume fraction of γ' to achieve better high-temperature properties than existing alloys, such as WASPALOY.* An alloy that has better high-temperature strength might also be expected to retain larger residual stresses when it is joined and be more resistant to subsequent postweld heat treatment.

*WASPALOY is a trademark of Precision Rings, Inc., Indianapolis, IN.

In this article, the magnitude of the residual stresses generated by inertia welding and the efficiency of subsequent post weld heat treatment in terms of stress relief is investigated for RR1000 by means of neutron-diffraction measurements. This technique enables the measurement of elastic strain in bulk materials *via* changes in lattice parameter, *a*. Unambiguous interpretation of lattice-parameter measurements in terms of elastic strain (and thereby stress) is, however, not straightforward. It was demonstrated in part I[1] that, under the extreme thermomechanical history experienced by the near-weld zone, marked changes in the local microstructure occur. Steep gradients in the volume fraction and size of primary (1 to 2 μm), intermediate secondary (70 to 300 nm), and tertiary (8 to 75 nm) γ' have been recorded. As a result, some repartitioning of the Ti/Al solute elements between γ and γ' can be expected. This may give rise to changes in the stress-free lattice spacing (a_0) across the near-weld region. Such changes can mistakenly be interpreted in terms of stress if they are not corrected for.

To date, there have been few reports on subsurface residual stress measurements of inertia welds. These have been either limited to the axial direction[2,3] or fail to include the a_0 issue.[4,5] Schroeder[6] has reported a maximum hoop stress of about 1000 MPa in an as-welded specimen (WASPALOY joined to IN 718*), when he applied a stress balance model. However, a_0 measurements were not reported. In this article, neutron diffraction data, corrected to account for variations in the stress-free lattice parameter, are reported. To achieve this, a_0 has been assessed as a function of axial distance from the weld line using a biaxial $\sin^2\psi$ method. The results from this direct measurement are compared with those calculated on the basis of axial stress balance. Stress measurements are reported for both as-welded and postweld heat treated (PWHT) specimens.

*IN718 is a trademark of INCO Alloys International, Inc., Huntington, WV.

II. EXPERIMENTAL

A. *Materials and Specimens*

The RR1000 material and the joints studied in this investigation have been described in part I.[1] In summary, two

M. PREUSS, Research Fellow, and P.J. WITHERS, Professor, are with the Manchester Materials Science Centre, University of Manchester and UMIST, Manchester M1 7HS, United Kingdom. Contact e-mail: michael.preuss@man.ac.uk J.W.L. PANG, Research Fellow, is with the Oak Ridge National Laboratory, Oak Ridge, TN 37830. G.J. BAXTER, Process Metallurgist, is with Rolls-Royce plc., Derby DE24 8BJ, United Kingdom.

Manuscript submitted November 19, 2001.

Table I. List of Specimens Measured at ISIS and ILL and Corresponding Samples from Part I;[1] the Postweld Heat Treatments of the Specimens were Carried out by Rolls-Royce plc

Specimen Condition	Diameter (mm)	Condition
S1	143	as welded
S2	143	conventional PWHT
S3	143	modified PWHT (+50 °C)
s1	50	as welded
s2	50	conventional PWHT
s3	50	modified PWHT (+50°C)
s4	50	modified PWHT (II) (+150°C)

inertia welds of outer diameter (OD) 143 mm and wall thickness 8 mm were provided by Rolls-Royce plc (Derby, United Kingdom). Both samples were welded under the same welding conditions. One specimen was examined in the as-welded condition (S1), and the other one was conventionally postweld heat treated (S2). After the first series of neutron diffraction measurements, S1 was given a modified PWHT that was 50 °C higher than S2. The code for this new condition is reported in this article as S3.

In addition to S1 through S3, four inertia-welded tubes of 50 mm OD were provided by Rolls-Royce plc. These specimens were welded with the same welding parameters (surface speed, inertia, and axial pressure) as S1 through S3 and are represented by s1 through s4. The heat-treatment conditions of all specimens are summarized in Table I.

Because of the relatively large neutron absorption coefficient of nickel, a neutron path length of 10 mm would reduce the diffracted beam intensity by ≈80 pct. To minimize the path length and facilitate the hoop strain measurements, a small window of 12 × 12 mm was electrodischarge machined from the weld region of S1 through S3 at a position distant from the neutron measurement location. A window was not feasible in s1 through s4 because of their small diameter.

To evaluate the extent of any variation in the stress-free lattice parameter, a_0, with axial distance from the weld in the as-welded and heat-treated conditions, two samples were cut out from a 143 mm OD sample that was welded with the same parameters as samples S1 and S2. The cutting plane was perpendicular to the hoop direction, and the dimensions of the slices were 15 × 8 × 0.5 mm^3 (axial × radial × hoop). One sample was PWHT in a tube furnace under argon atmosphere at the same temperature as S2 and subsequently air cooled. Thin slices were then machined from the two samples, ground, and electropolished to remove machine-induced stresses at the surface.

B. *Neutron Diffraction Measurements*

All measurements of S1 through S3 were carried out on the ENGIN diffractometer at the ISIS neutron spallation source, Rutherford Appleton Laboratory (Chilton, UK). At pulsed neutron sources, neutrons of all wavelengths emerge over a short-time pulse from the source. With detectors placed at a given angle, due to time of flight, the whole diffraction profile can be recorded as a function of time.[7] The orientation of the specimens with respect to the neutron

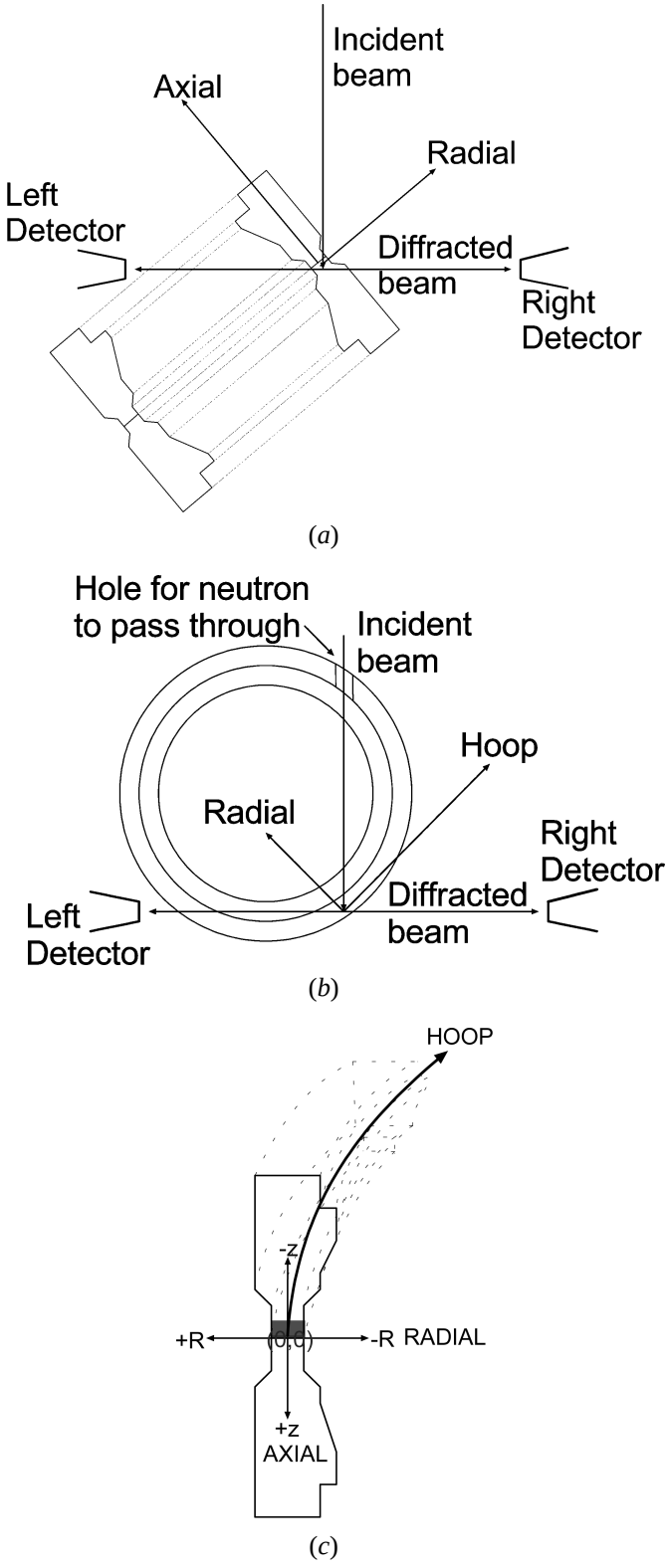

Fig. 1—Alignment of the specimen with respect to the neutron beam in order to measure the three principal axes.

beam is shown in Figures 1(a) and (b). The direction of the strain measurement is parallel to the scattering vector, **Q**, which is the bisector of the incident and diffracted neutron beams. The presence of two detector banks ±90 deg apart means that the strains along two perpendicular sample directions can be measured simultaneously. The sampling gage

Table II. Gage Volumes Used during the Neutron Diffraction Measurements as a Function of the Measurement Direction

Location	Strain Direction	Gage Volume (mm)
ISIS	radial	10 × 1 × 1.5
ISIS	axial	10 × 1 × 1.5
ISIS	hoop	2 × 1 × 1.5
ILL	hoop	2 × 2 × 1

volume is defined by the intersection of the incident and diffracted beams. The lattice parameter, a, of the lattice planes with plane normal parallel to **Q**, averaged over the correctly oriented grains within the sampling volume, was determined by Rietveld refinement of the spectra.[8]

The lattice spacing was mapped out over a plane at a specific hoop location for S1 through S3 between the weld line and up to 8 mm away from it. A previous experiment at Risø (Denmark)[9] had indicated that the residual stresses in a similar weld were essentially symmetric about the weld line ($z = 0$). Consequently, measurements were only made on one-half of the coordinate system ($z + ve$). The sample coordinate system, as defined for the experiment, is shown in Figure 1(c).

All measurements on s1 to s4 were performed at the Institute Laue-Langevin (ILL) high-flux reactor in Grenoble, France. The purpose of these measurements was to determine an optimum temperature for a modified postweld heat treatment. Because of a long counting time (up to 3 hours/point), only the hoop strains close to the inner diameter were studied because this is the area where the most significant stresses were expected. This was carried out with the same orientation of the specimens and direction of the scattering vector, **Q**, as described for the ISIS experiment. The wavelength employed at the ILL was $\lambda = 2.99$ Å. Using the (111) reflection of Ni, a scattering angle of about $2\theta = 92$ deg was obtained, resulting in a virtually cuboidal gage volume (Table II), as used on ENGIN. This *hkl* reflection has been shown by Stone *et al.*[10] to be essentially insensitive to plastic anisotropy.

The strain for all measurements was calculated using

$$\varepsilon = \frac{d - d_0}{d_0} = \frac{a - a_0}{a_0} \qquad [1]$$

where d_0 is the stress-free lattice spacing (ILL) and a_0 (ISIS) is the stress-free lattice parameter. The preliminary nominal, stress-free lattice spacing was generally determined by a far-field measurement for each sample.

The corresponding axial, radial, and hoop residual stress fields for S1, S2, and S3 were calculated using

$$\sigma_{\text{axial}} = \frac{\text{E}}{(1 + \nu)(1 - 2\nu)} [(1 - \nu)\varepsilon_{\text{axial}} + \nu(\varepsilon_{\text{radial}} + \varepsilon_{\text{hoop}})], \textit{ etc.} \qquad [2]$$

where E is the bulk Young's modulus, and ν is Poisson's ratio. As only the strain in the hoop direction of s1 to s4 was measured, the residual stress in these specimens were not determined.

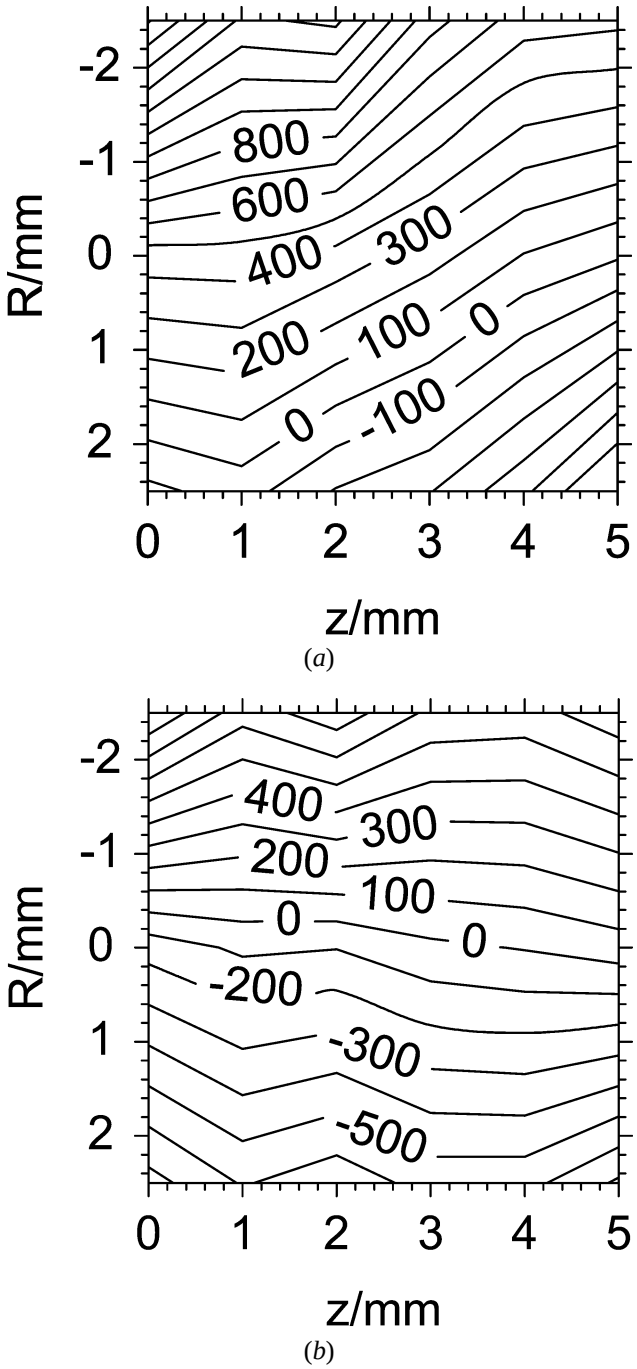

Fig. 2—(*a*) Uncorrected nominal (constant a_0) and (*b*) corrected ($a_0(z)$) axial residual stress field (in MPa) in S1.

C. *High-Energy Synchrotron X-ray Measurements*

Thin radial-axial plane slices were cut from an inertia welded 143 mm OD specimen as described in part I.[1] These slices were measured in transmission on beam-line ID11 at the European Synchrotron Radiation Facility (Grenoble, France). Monochromatic X-rays of 60 ke V (0.203 Å) were used. A slit size of 150 μm in the axial and 3 mm in the radial direction was used, centered at $R = 0$ and scanned along the z direction. The (111), (200), (220), and (311) primary reflections of the γ matrix and the γ' phase were measured together with the (100) superlattice reflection of

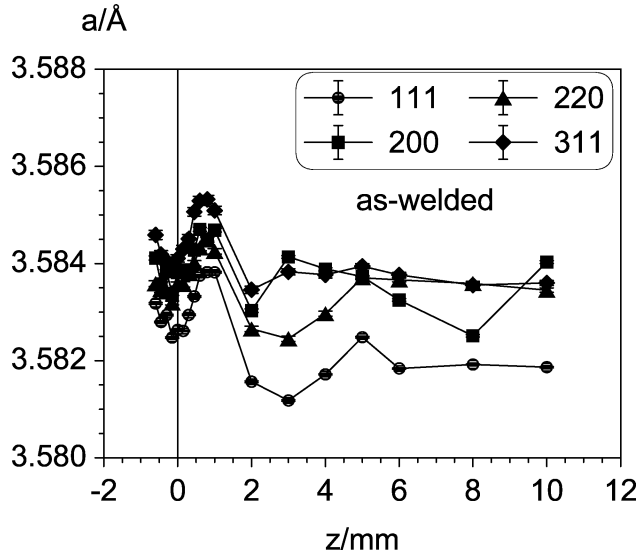

Fig. 3—The axial lattice parameter measured using four diffraction peaks ((111), (200), (220), and (311)) for a thin slice in the as-welded condition (S1) on ID11.

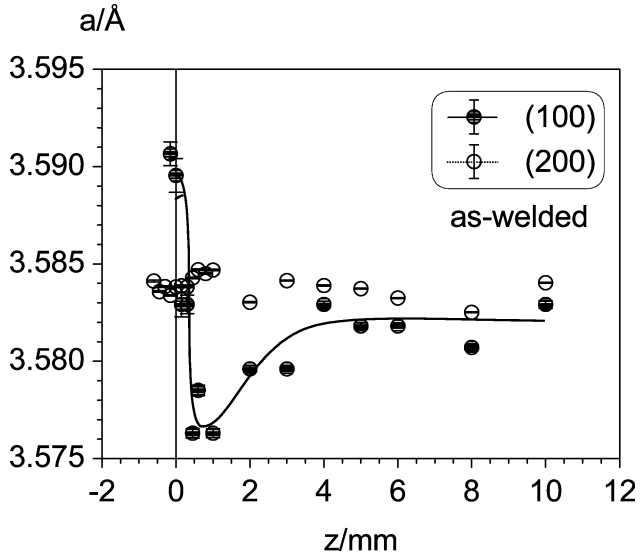

Fig. 4—The variation in axial lattice parameter with distance from the weld line of the (100) γ' superlattice reflection and the (200) ($\gamma + \gamma'$) reflection of the as-welded sample (S1) measured on beam line ID11.

the γ' phase. The measurement time of a primary reflection was in the range of seconds, whereas the measurements of the γ' superlattice peak took up to 45 minutes per point. Because of the 0.5 mm thickness of the slices, the beam bathed a statistically sufficient number of grains during the scanning of the samples.

D. *Laboratory X-ray Measurements*

The lattice parameter, a_3 (scattering vector, **Q**, perpendicular to the surface), across the weld line was measured with a small step size of 0.25 mm and at three radial positions ($R = -2.5$, 0, and 2.5) using a laboratory X-ray source. In addition, $\sin^2 \psi$ measurements were performed for $R = 0$ in the two principal in-plane stress directions. The X-ray diffractometer used was a Bruker AXS D8 Discover (Bruker AXS, Ltd., Congleton, U.K.), which has a polycapillary optics X-ray beam and a two-dimensional area detector collecting backscattered X-ray Debye–Scherrer cones. An iron-anode X-ray tube was used, and measurements were made on the (311) diffraction peak. The sample was correctly positioned for each measurement point by using of a video microscope and a locating laser, which is positioned 45 deg to the microscope. The (311) diffraction peak was recorded at a 2θ angle of about 128 deg with an irradiated area of approximately 1 mm^2. The time taken for one measurement point was 5 minutes.

At the low surface penetration typical of lab full stage X-rays into nickel (15 μm), an in-plane biaxial stress field ($\sigma_3 = 0$) can be assumed. Using the $\sin^2 \psi$ technique to measure the principal inplane stresses, σ_1 and σ_2, then allows determination of $d_{\phi\psi}$ and $d_{\phi'\psi}$ with $\phi' = \phi + 90$ deg and $\phi = 0$ corresponding to the direction of σ_1. A more detailed description of the biaxial $\sin^2 \psi$ technique and the determination of d_0 in a biaxial stress field can be found in References 11 and 12. The term d_0 can then be determined using

$$d_0 = \frac{\nu}{1+\nu} \cdot \frac{d_{\phi\psi} + d_{\phi'\psi} - 2d_{\perp}}{\sin^2\psi} + d_{\perp} \qquad [3]$$

where Poisson's ratio, ν, is 0.27 for the (311) plane.

III. RESULTS AND DISCUSSION

A. *Stress Balance*

Figure 2(a) shows a contour map of the preliminary axial residual stress field calculated using Eq. [1] and [2], assuming a nominal stress-free lattice parameter a_0 (constant across the weld line). The contour map was calculated from 12 measurement points. The average uncertainty in the calculated residual stresses was around ± 60 MPa. Equilibrium in a tubular structure requires that the axial stress should be balanced when considered over the wall thickness (the radial direction). Figure 2(a) shows that the uncorrected nominal axial stress in the area close to the weld line ($z = 0$) is in tension close to the inner diameter ($R = -4$) and that this is not counterbalanced by a comparable compressive stress close to the OD ($R = 4$). Further from the weld line ($z = 5$), stress balance is more nearly observed in the uncorrected values. This is to be expected considering the more modest thermal excursion experienced there. Clearly, the stress-free lattice spacing near the weld has been underestimated resulting in an apparent net tensile stress. By adjusting a_0 as a function of axial position, it is possible to ensure the balance of axial stress, and the corrected results are shown in Figure 2(b). To achieve this, an inferred variation in a_0 equivalent to an 800 microstrain error is required. This has resulted in essentially horizontal stress contours. Failure to correct the stress-free lattice spacing in the vicinity of the weld would also lead to large errors in the inferred radial and hoop stresses. In fact, on the weld line, the error in the hoop direction is around $+600$ MPa, which is a significant fraction of the yield stress ($\sim$1050 MPa).

B. *Lattice Parameter Determination using High-Energy X-rays*

Given the large error that would be introduced by a failure to compensate for a variation in the stress-free lattice spacing as a function of position, it is important to corroborate the inferred $a_0(z)$ variation determined in Section II, D. In

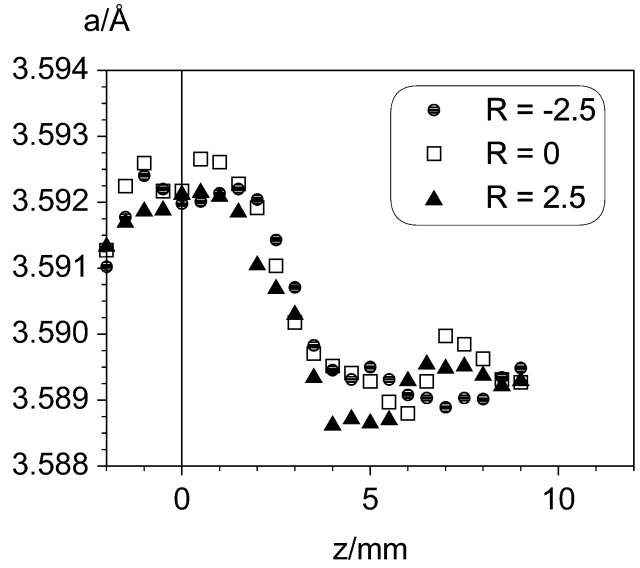

Fig. 5—The a_3 profiles measured at three different radial positions for (S1) on a laboratory X-ray machine.

part I,[1] the behavior of major and superlattice reflections was reported from thin weld slices using synchrotron X-ray diffraction. While the slices are not strictly stress-free, variations in the stress-free lattice parameter, a_0, would be expected to be evident in the results. Figure 3 shows the lattice parameters determined from four diffraction peaks in the as-welded condition measured at the synchrotron beam line ID11. The slices were measured in transmission with the radial and axial direction of the slices perpendicular to the incident beam. It can be seen that the profiles of all four reflections are very similar, which indicates that intergranular stress is not responsible for the overall shift in *a*. In the area between 0.5 and 2 mm from the weld line, a steep increase in the lattice parameter is observed that is of the same order of magnitude as the change required to achieve stress balance (as previously discussed). However, exactly at the weld line, the lattice parameter falls to a value close to the values measured in the parent material.

In addition to the main γ reflections, the (100) γ' superlattice reflection was measured (Figure 4). The as-welded sample displays a dramatic rise in the (100) γ' lattice parameter close to the weld line, which is equivalent to 4000 microstrain. When compared to the (200) reflection, the (100) reflection clearly varies in the opposite direction. This suggests the presence of interphase microstresses or radical changes in element partitioning in the near-weld region. However, they are not exactly balanced because the (200) reflection consists of the (200) γ and (200) γ' peak, which cannot be deconvolved. Because of the steep temperature gradients introduced in the near-weld region, different maximum temperatures are experienced as a function of axial position during the welding process. With rising maximum temperature, an increasing element partitioning effect between the matrix and the coherent precipitates might be expected, which could explain the shift of *a*. Indeed, Blavette *et al.*[13] investigated the precipitation of γ' phase in nickel-based superalloys by atom-probe techniques and showed that coarse and finer γ' formed at different temperature ranges and have different levels of aluminum and titanium content. Exactly at the weld line, a_{100} rises sharply (Figure 4). In part I,[1] it was shown that, at the weld line, all γ' had been in solution during the welding process. Only very fine, tertiary γ' was observed, and this supports the assumption that significant supercooling took place before γ' began to precipitate. Consequently, in the as-welded condition, γ' at the weld line has a different chemical composition to that of the parent material and, thus, a different lattice parameter, *a*.

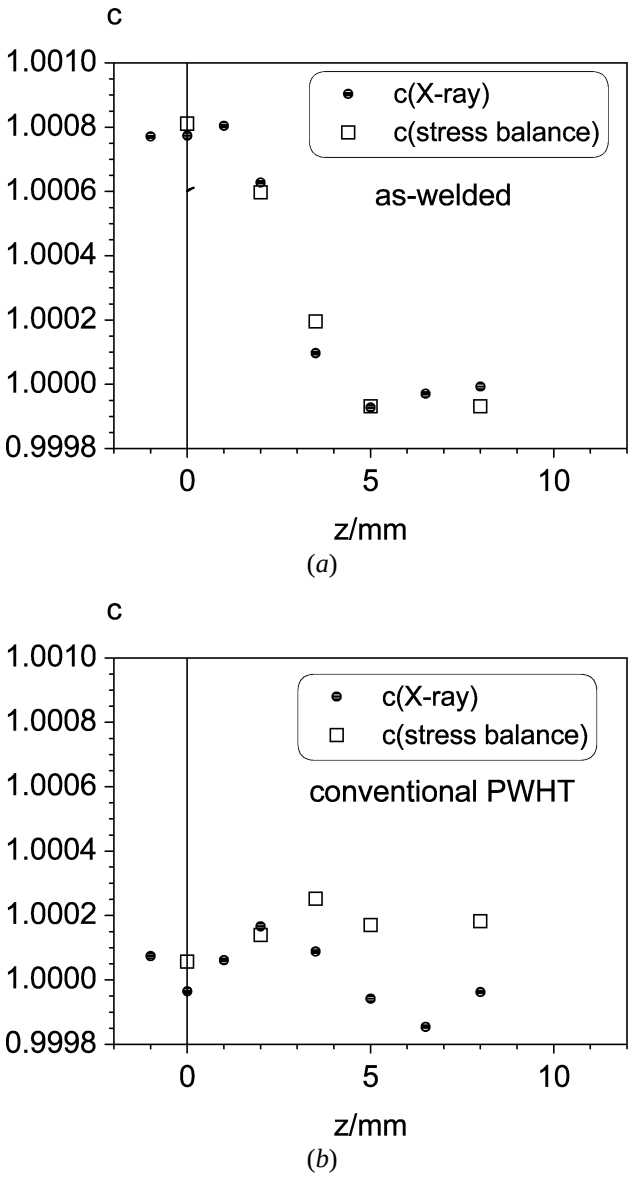

Fig. 6—Correction factor $a_0(z) = c(z)\ a_0(\text{parent})$ calculated on the basis of imposing stress balance on the axial measurements for the as-welded condition and as determined from laboratory X-ray measurement for (*a*) the as-received weld (S1) and (*b*) the conventional PWHT (S2).

C. *Conventional Laboratory X-ray Measurements*

The same slices used for the synchrotron measurement were also used for conventional X-ray measurements. The lattice parameter, a_3, determined from the (311) reflection using a laboratory X-ray diffractometer, is plotted for the as-welded sample against the axial position in Figure 5.

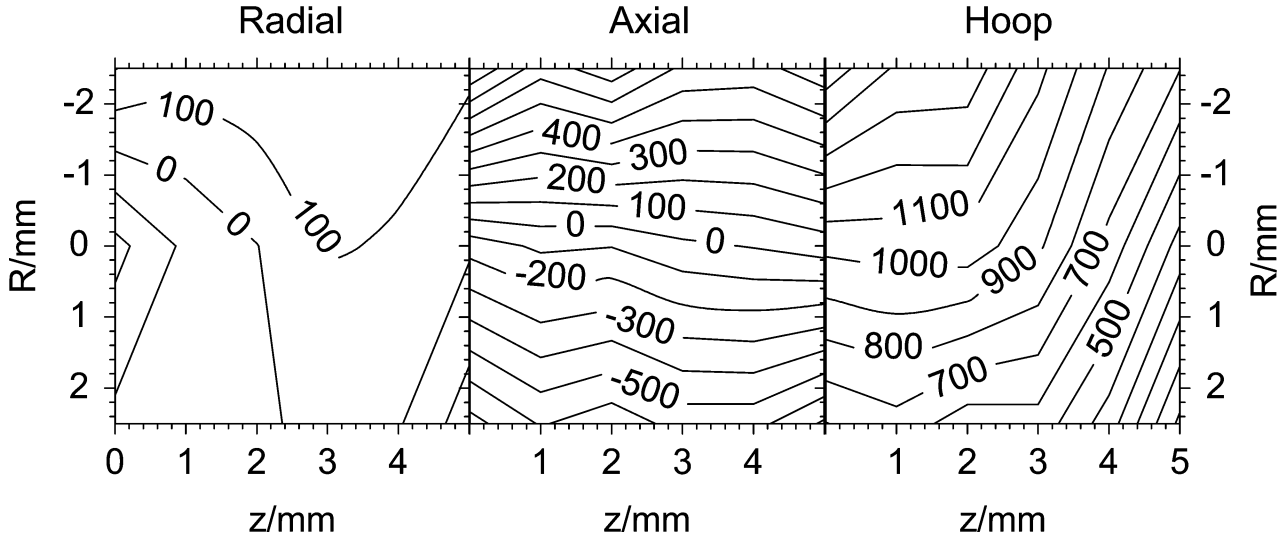

Fig. 7—Map of residual stress field (in MPa) of S1 (as-welded) with an axially variant stress-free lattice parameter.

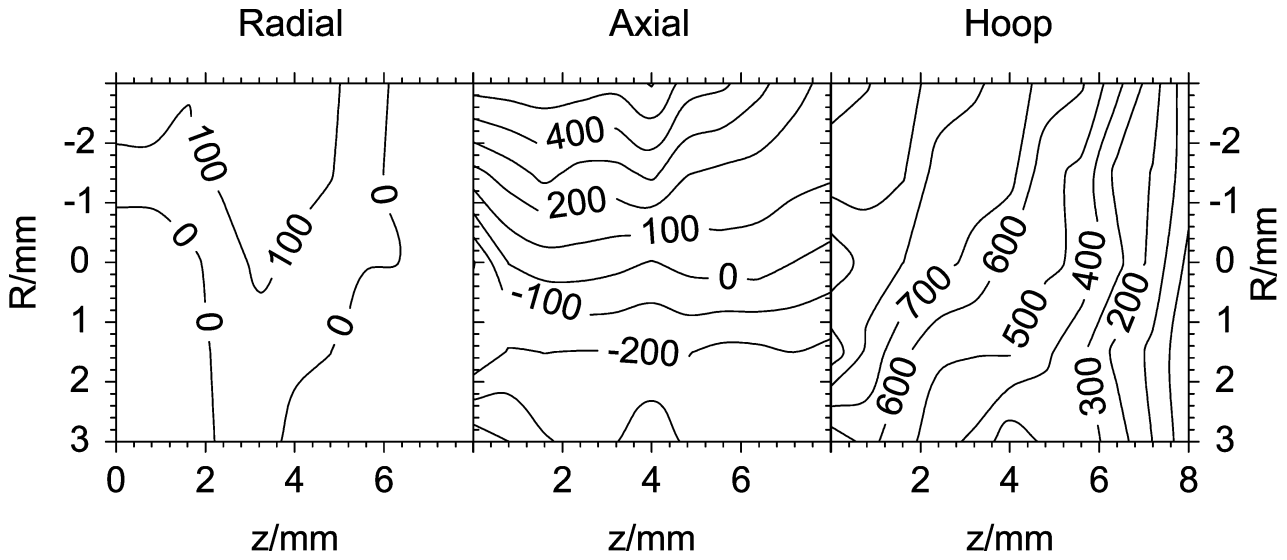

Fig. 8—Map of residual stress field (in MPa) of S2 (conventional PWHT) using an axially invariant stress-free lattice parameter.

The measurements were performed at three different radial positions to detect any changes in lattice parameter in the radial direction (this was assumed to be negligible for the stress balance approach). As can be seen, the observed variation is essentially independent of radial position. Consequently, a_0 can be taken to vary only as a function of axial position and validates the assumption that underpins the stress balance approach. This is not totally unexpected because the thermal history experienced by the weld region is known to vary sharply with *z* but weakly with *R*. The lattice parameter calculated from the (311) reflection here has a similar profile across the weld line to that observed during the synchrotron X-ray measurements. It has to be noted that, in the 60 keV high-energy synchrotron X-ray experiment (through slice thickness), the lattice parameters were measured in the axial (in-plane) direction, whereas using the 8 keV ($\approx$15 μm penetration) laboratory X-ray source, the hoop (out-of-plane) direction was measured. The drop of the lattice parameter at the weld line in the former is hardly detectable in the laboratory X-ray measurement because of the larger spot size in the axial direction of the X-ray machine (1 mm^2) compared to ID11 (150 μm). However, the X-ray beam size of the laboratory machine is comparable to the gauge size of the axial direction during neutron diffraction experiments at ISIS.

The lattice parameter, a_3, should not be used to determine the stress-free lattice parameter across the weld line. Although small slices were used for these measurements, the slices are not stress free. However, because of the shallow penetration of the X-rays and the limited thickness of the slices (0.5 mm), a biaxial stress field ($\sigma_3 = 0$) can be assumed.

To take the biaxial stress field into account while determining a_0, a rigorous biaxial $\sin^2 \psi$ measurement was carried out. The a_0 measurements were used to calculate a correction factor, ($a_0(z) = c(z) \bullet a_0$(parent)), by normalizing the meas-

ured values by the stress-free lattice parameter obtained in the parent material. Figure 6(a) shows the variation in the correction factor against axial distance from the weld line obtained from the biaxial $\sin^2 \psi$ measurement and that inferred from the stress-balanced model. As can be seen, excellent agreement for the as-welded sample was obtained between both a_0 correction methods, which justifies the simple method of balancing the axial stress to account for the axial variation in a_0 when determining the stress state.

The change of a_0 across the weld line in S2 was also measured by the biaxial $\sin^2 \psi$ method. Figure 6(b) compares the correction factor against the axial position obtained from the biaxial $\sin^2 \psi$ measurement and the forced stress balance model. Both methods suggest that no significant chemical (stress-free) variation of a_0 is detectable with distance from the weld line. This is perhaps to be expected given the extended time at the elevated temperature for chemical repartitioning between γ and γ'. As a result, the strain and stresses can be directly calculated from the stress-free lattice parameter measured on the parent material during the neutron diffraction experiment.

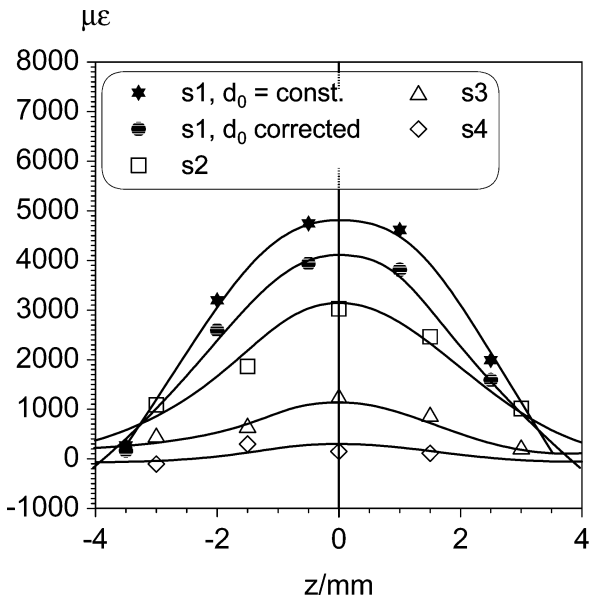

Fig. 9—Hoop strain (in 10^{-6}) recorded at $R = -2.5$ of the 50 mm diameter variously heat-treated specimens measured at ILL.

D. *Residual Stresses*

Given that a reliable point-by-point measure of the stress-free lattice parameter is obtained, the residual strains and stresses in the as-welded and PWHT samples can be calculated. Figure 7 shows the residual stress field of S1 with the axial stress forced into balance by correcting a_0 for each axial position. The maximum residual stress is in the range of 1500 MPa and can be observed in the hoop direction close to the inner diameter ($R = -4$). The axial residual stress field exhibits a significant bending moment, which indicates that either the tooling or uneven heating also plays a key role during the welding process.[9] As one would expect, the radial stress component is negligible across the weld line because of the short distance between the inner and outer diameter. The uncorrected residual stress maps have been published previously[5] and comparison of the results shows the significance of the a_0 correction. When the chemical shift of a_0 is not taken into account, residual stresses close to the weld line are overestimated (by 600 MPa).

In Figure 8, the residual stress field is plotted for S2. The contour maps were calculated from 20 measurement positions with an average stress uncertainty of ± 60 MPa. The variations in the three components of the residual stress field are very similar to S1, except that the stress magnitudes are reduced by about 30 pct. The maximum stress in the hoop direction is around 1000 MPa in S2. As already shown, the axial stresses in radial direction are close to stress balance in the PWHT specimen without invoking an axially variant lattice parameter. This justifies the direct use of the stress-free lattice parameter obtained from the far-field measurements during the neutron diffraction experiment.

The measurement of S2 has shown that the conventional postweld heat treatment is not completely effective. In Figure 9, the hoop strain against the axial position near the key inner-radius location ($R = -2.5$) is plotted for specimens s1, s2, s3, and s4 measured at the ILL in Grenoble. The

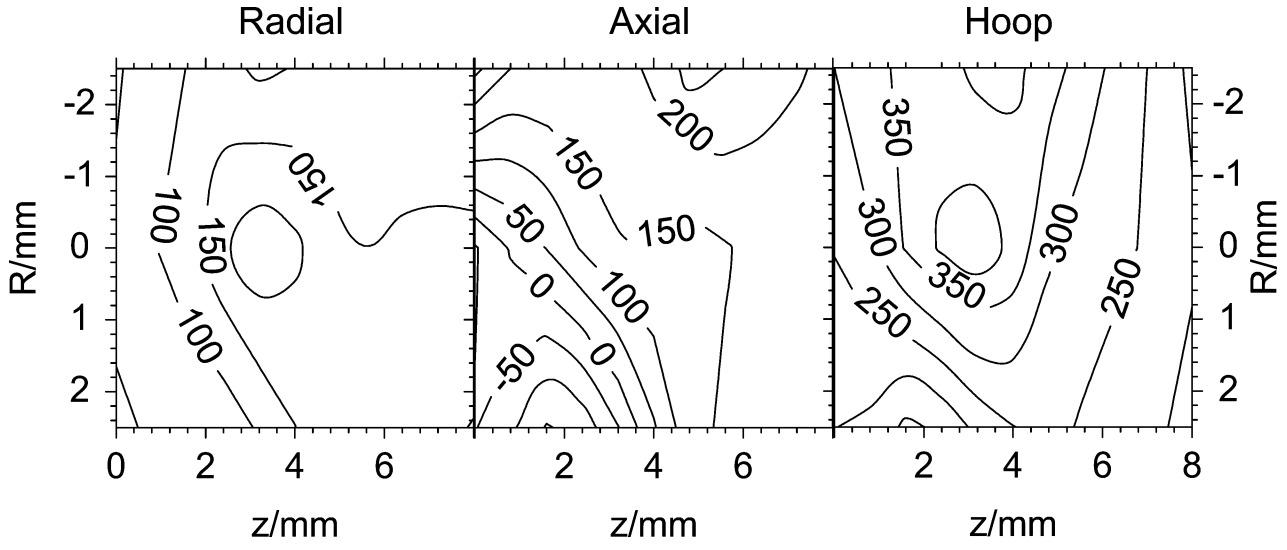

Fig. 10—Map of residual stress field (in MPa) of S3 (modified postweld heat treatment).

measured strain for s1 is plotted using the constant and the axially variant corrected a_0 values. For the correction of a_0, the $c(z)$ factors from the 143-mm diameter specimen were used. When the strains of s1 (a_0 corrected) are compared with s2, a 25 pct reduction in strain is apparent and in good agreement with the measurements of S1 and S2. A 50 °C rise in PWHT (s3) reduces the hoop strain significantly (75 pct). When heat treated at a temperature of 150 °C above the conventional heat-treatment temperature, s4, the hoop strain is completely relieved. The pronounced reduction in hoop strain in s3 led to the +50 °C heat treatment of the 143 mm specimen (S3) to measure all three principal directions and to calculate the residual stress field. Figure 10 shows the contour maps for S3 calculated from 15 measurement points with an average stress uncertainty of ±60 MPa. It can be seen that the stresses in the axial and hoop direction are significantly lower than in S1 and S2. The maximum stress in the hoop direction is less than 400 MPa. The axial stresses, which were significant in S1 have also been largely relieved. It is also interesting to note that the hoop stresses in S3 at the inner and outer diameter are very similar, whereas in the other two conditions this was not the case.

IV. SUMMARY AND CONCLUSIONS

The residual stresses in the as-welded (S1), conventional (S2), and modified heat-treated (S3) RR1000 inertia welds have been mapped. RR1000 is a high-strength nickel-based superalloy containing a volume fraction of almost 50 pct γ', when fully annealed. In addition to the stress-field measurements by means of neutron diffraction, we have studied the variation of a_0 across the weld line using a combination of synchrotron radiation and a laboratory X-ray source. The conclusions can be summarized as follows.

1. When the residual stress field for as-welded specimens is calculated from strain measurements (on the basis of a constant a_0 evaluated from far-field measurements) the tensile residual stresses close to the weld line are overestimated because of a chemical shift (increase) of a_0 in the heat-affected zone.
2. The chemical-induced increase in a_0 in the as-welded condition is due to an element-partitioning effect between γ and γ' in the heat-affected zone. This is evidenced by the shift of the (100) superlattice reflection and the (200) reflection in opposite directions.
3. To determine the correct a_0 shift in the axial direction, a biaxial $\sin^2 \psi$ measurement was carried out. This technique enabled us to take into account the residual stresses in thin slices when determining a_0. The measured shift of a_0 with position was invariant with radial position. As a result, it was in excellent agreement with the a_0 shift calculated from the stress balance correction. A significant shift of a_0 was only observed in the as-welded sample, whereas the a_0 shift in the PWHT sample can be neglected.
4. The residual stresses introduced during welding are very large. The maximum tensile stress close to the inner diameter in the hoop direction is ≈1500 MPa. Tooling also plays a key role in the development of residual stresses as inferred from the large axial stresses in the welds.
5. The conventional postweld heat treatment relieves the residual stresses only to a limited extent. The maximum stress is still in the range of 1000 MPa for the hoop component.
6. Increasing the postweld heat treatment temperature by 50 °C led to a pronounced reduction of the axial and hoop stresses. The maximum hoop stress observed does not exceed 400 MPa. The large differences between the inner and outer diameter stresses of the hoop component have vanished.

ACKNOWLEDGMENTS

The authors thank Dr. M.R. Daymond and J. Wright (ISIS, ENGIN), Dr. A. Terry and Dr. G. Vaughan (ESRF, ID11), Dr. T. Pirling (ILL), and Judith Shackleton (MMSC) for experimental assistance and Peter Wilson, Kevin Bass, and A. Thompson (Rolls-Royce plc.) for advice. These experiments were performed under EPSRC Project No. GR/M68704 and are financially supported by EPSRC and Rolls-Royce plc.

REFERENCES

1. M. Preuss, J.W.L. Pang, P.J. Withers, and G. Baxter: *Metall. Mater. Trans. A*, 2002, vol. 33A, pp. 3215-25.
2. H.G. Priesmeyer and J. Schroeder: *Residual Stresses—III: Science and Technology*, H. Fujiwara, T. Abe, and K. Tanaka, eds., Elsevier Applied Science, London, 1992, pp. 253-58.
3. M.E. Abdel Moniem, S.M. Serag, A.A. Nasses, and A.A. Moustafa: *Wear*, 1981, vol. 70, pp. 227-41.
4. H.U. Baron: *3rd Int. Conf. on welding in Aerospace Industry*, German Welding Society, Essen, 1993, pp. 114-17.
5. J.W.L. Pang, M. Preuss, P.J. Withers, and G.J. Baxter: *6th Conf. on residual stresses (ICRS-6)*, IOM Communication, London, 2000, pp. 1415-21.
6. J. Schroeder: Ph.D. Thesis, Technische Universitaet Hamburg-Harburg, Hamburg, 1993, p. 119.
7. M.W. Johnson, L. Edwards, and P.J. Withers: *Physica B*, 1997, vol. 234, pp. 1141-43.
8. R.A. Young: *Rietveld Method*, Oxford University Press, Oxford United Kingdom, 1993.
9. J.W.L. Pang, G.J. Baxter, P.J. Withers, G. Rauchs, and M. Preuss: Oak Ridge National Lab., Oak Ridge, TN, unpublished research, 2001.
10. H.J. Stone, T.M. Holden, and R.C. Reed: *Scripta Mater.*, 1999, vol. 40, pp. 353-58.
11. I.C. Noyan and J.B. Cohen: *Residual Stress, Measurement by Diffraction and Interpretation*, Springer-Verlag, Berlin, 1987, pp. 122-25.
12. L. Edwards, J. Santisteban, M.E. Fitzpatrick, G. Bruno, A. Steuver, P.J. Withers, M.R. Daymond, and M.W. Johnson: *6th Conf. on Residual Stresses (ICRS-6)*, IOM Communication, London, 2000, pp. 1239-46.
13. D. Blavette, A. Bostel, and J.M. Sarrau: *Metall. Trans. A*, 1985, vol. 16A, pp. 1703-11.